Investigating the thermal environment effects on geometrically nonlinear vibration of smart functionally graded plates [†]

Farzad Ebrahimi[*], Abbas Rastgoo and Mansoor Nikkhah Bahrami

Department of Mechanical Engineering, University of Tehran, Tehran, Iran

---

Abstract

An analytical solution for a sandwich circular FGM plate coupled with piezoelectric layers under one-dimensional heat conduction is presented. All materials of the device may be of any functional gradients in the direction of thickness. The solution exactly satisfies all the equilibrium conditions and continuity conditions for the stress, displacement and electric displacement as well as electric potential on the interfaces between adjacency layers. A nonlinear static problem is solved first to determine the initial stress state and pre-vibration deformations of the FG plate that is subjected to in-plane forces and applied actuator voltage in thermal environment in the case of simply supported boundary conditions. By adding an incremental dynamic state to the pre-vibration state, the differential equations that govern the nonlinear vibration behavior of pre-stressed piezoelectric coupled FGM plates are derived. The role of thermal environment as well as control effects on nonlinear static deflections and natural frequencies imposed by the piezoelectric actuators using high input voltages are investigated. Numerical examples are provided and simulation results are discussed. Numerical results for FGM plates with a mixture of metal and ceramic are presented in dimensionless forms. The good agreement between the results of this paper and those of the finite element (FE) analyses validated the presented approach. In a parametric study the emphasis is placed on investigating the effect of varying the applied actuator voltage and thermal environment as well as gradient index of FG plate on the dynamics and control characteristics of the structure.

Keywords: Functionally graded material; Nonlinear vibration analysis; Piezoelectric actuators

---

1. Introduction

The concept of developing smart structures has been extensively used for active control of flexible structures during the past decade [1-3]. In this regard, the use of axisymmetric piezoelectric actuators in the form of a disc or ring to produce motion in a circular or annular substrate plate is common in a wide range of applications including micro-pumps and micro-valves [4, 5], devices for generating and detecting sound [6] and implantable medical devices [7]. They may also be useful in other applications such as microwave micro-switches where it is important to control distortion due to intrinsic stresses [8]. Functionally graded materials (FGMs) are a new generation of composite materials wherein the material properties vary continuously to yield a predetermined composition profile. These materials have been introduced to benefit from the ideal performance of its constituents, e.g., high heat/corrosion resistance of ceramics on one side, and large mechanical strength and toughness of metals on the other side. FGMs have no interfaces and are hence advantageous over conventional laminated composites. FGMs also permit tailoring of material composition to optimize a desired characteristic such as minimizing the maximum deflection for a given load and boundary conditions, or maximizing the first frequency of free vibration, or minimizing the maximum principal tensile stress. As a result, FGMs have gained potential applications in a wide variety of engineering components or systems, including armor plating, heat engine components and human implants.

FGMs are now developed for general use as structural components and especially to operate in environments with extremely high temperatures. Low thermal conductivity, low coefficient of thermal expansion and core ductility have enabled the FGM materials to withstand higher temperature gradients for a given heat flux. Structures made of FGMs are often susceptible to failure from large deflections, or excessive stresses that are induced by large temperature gradients and/or mechanical loads. It is therefore of prime importance to account for the geometrically nonlinear deformation as well as the thermal environment effect to ensure more accurate and reliable structural analysis and design.

Also in recent years, with the increasing use of smart material in vibration control of plate structures, the mechanical response of FGM plates with surface-bonded piezoelectric layers has attracted some researchers' attention. Since this area is relatively new, published literature on the free and forced vibration of FGM plates is limited and most are focused on the cases of the linear problem. Among those, a 3-D solution for rectangular FG plates coupled with a piezoelectric actuator layer was proposed by Reddy and Cheng [9] using transfer matrix and asymptotic expansion techniques. Wang and Noda [10] analyzed a smart FG composite structure composed of a layer of metal, a layer of piezoelectric and an FG layer in between, while He et al. [11] developed a finite element model for studying the shape and vibration control of FG plates integrated with piezoelectric sensors and actuators. Yang et al. [12] investigated the nonlinear thermo-electro-mechanical bending response of FG rectangular plates that are covered with monolithic piezoelectric actuator layers on the top and bottom surfaces of the plate. More recently, Huang and Shen [13] investigated the dynamics of an FG plate coupled with two monolithic piezoelectric layers at its top and bottom surfaces undergoing nonlinear vibrations in thermal environments. In addition, finite element piezothermoelasticity analysis and the active control of FGM plates with integrated piezoelectric sensors and actuators was studied by Liew et al. [14] and the temperature response of FGMs using a nonlinear finite element method was studied by Zhai et al. [15]. All the aforementioned studies focused on the rectangular-shaped plate structures. To the authors' best knowledge, no researches dealing with the nonlinear vibration characteristics of the circular functionally graded plate integrated with the piezoelectric layers have been reported in the literature except the author's recent works in presenting an analytical solution for the free axisymmetric linear vibration of piezoelectric coupled circular and annular FGM plates [16-20] and investigating the applied control voltage effect on piezoelectrically actuated nonlinear FG circular plate [21] in which the thermal environment effects are not taken in to account.

Consequently, a non-linear dynamics and vibration analysis is conducted on pre-stressed piezo-actuated FG circular plates in thermal environment. Nonlinear governing equations of motion are derived based on Kirchhoff's-Love hypothesis with von-Karman type geometrical large nonlinear deformations. Dynamic equations and boundary conditions including thermal, elastic and piezoelectric couplings are formulated and solutions are derived. An exact series expansion method combined with perturbation approach is used to model the nonlinear thermo-electro-mechanical vibration behavior of the structure. Numerical results for FG plates with various mixture of ceramic and metal are presented in dimensionless forms. A parametric study is also undertaken to highlight the effects of the thermal environment, applied actuator voltage and material composition of FG core plate on the nonlinear vibration characteristics of the composite structure. The new features of the effect of thermal environment and applied actuator voltage on free vibration of FG plates and some meaningful results in this paper are helpful for the application and the design of nuclear reactors, space planes and chemical plants, in which functionally graded plates act as basic elements.

2. Functionally graded materials (FGM)

Nowadays, not only can FGM easily be produced but one can control even the variation of the FG constituents in a specific way. For example in an FG material made of ceramic and metal mixture, we have:

$$V_m + V_c = 1 \tag{1}$$

in which V_c and V_m are the volume fraction of the ceramic and metallic part, respectively. Based on the power law distribution [22], the variation of V_c vs. thickness coordinate (z) with its origin placed at the middle of thickness, can be expressed as:

$$V_c = (z/h_f + 1/2)^n, \quad n \geq 0 \tag{2}$$

in which h_f is the FG core plate thickness and n is the FGM volume fraction index. Note that the variation of both constituents (ceramics and metal) is linear when $n=1$. We assume that the inhomogeneous material properties, such as the modulus of elasticity E, density ρ, thermal expansion coefficient α and the thermal conductivity κ change within the thickness direction z based on Voigt's rule over the whole range of the volume fraction [23] while Poisson's ratio υ is assumed to be constant in the thickness direction [24] as:

$$E(z) = (E_c - E_m)V_c(z) + E_m$$
$$\rho(z) = (\rho_c - \rho_m)V_c(z) + \rho_m$$
$$\kappa(z) = (\kappa_c - \kappa_m)V_c(z) + \kappa_m$$
$$\alpha(z) = (\alpha_c - \alpha_m)V_c(z) + \alpha_m$$
$$v(z) = v \tag{3}$$

where subscripts m and c refer to the metal and ceramic constituents, respectively. After substituting Vc from Eq. (2) into Eqs. (3), material properties of the FGM plate are determined in the power law form-the same as those proposed by Reddy and Praveen [22]:

$$E_f(z) = (E_c - E_m)(z/h_f + 1/2)^n + E_m$$
$$\rho_f(z) = (\rho_c - \rho_m)(z/h_f + 1/2)^n + \rho_m$$
$$\kappa_f(z) = (\kappa_c - \kappa_m)(z/h_f + 1/2)^n + \kappa_m$$
$$\alpha_f(z) = (\alpha_c - \alpha_m)(z/h_f + 1/2)^n + \alpha_m \tag{4}$$

3. Thermal environment

Assume a piezo-laminated FGM plate is subjected to a thermal environment and the temperature variation occurs in the thickness direction and 1D temperature field is assumed to be constant in the r-θ plane of the plate. In such a case, the temperature distribution along the thickness can be obtained by solving a steady-state heat transfer equation

$$-\frac{d}{dz}\left[\kappa(z)\frac{dT}{dz}\right]=0 \tag{5}$$

in which

$$\kappa(z)=\begin{cases}\kappa_p & \left(h_f/2 < z < h_p + h_f/2\right)\\ \kappa_f(z) & \left(-h_f/2 < z < h_f/2\right)\\ \kappa_p & \left(-h_p - h_f/2 < z < -h_f/2\right)\end{cases} \tag{6}$$

$$T(z)=\begin{cases}T_p(z) & \left(h_f/2 \le z \le h_p + h_f/2\right)\\ T_f(z) & \left(-h_f/2 \le z \le h_f/2\right)\\ \widetilde{T}_p(z) & \left(-h_p - h_f/2 \le z \le -h_f/2\right)\end{cases} \tag{7}$$

where κ_p and κ_f are the thermal conductivity of piezoelectric layers and FG plate, respectively. Eq. (5) is solved by imposing the boundary conditions as

$$T_p\big|_{z=h_p+h_f/2}=T_U \, , \, \widetilde{T}_p\big|_{z=-h_p-h_f/2}=T_L \tag{8}$$

and the continuity conditions

$$T_p\big|_{z=h_f/2}=T_f\big|_{z=h_f/2}=T_1$$

$$T_f\big|_{z=-h_f/2}=\widetilde{T}_p\big|_{z=-h_f/2}=T_2$$

$$\kappa_p\frac{dT_p(z)}{dz}\bigg|_{z=h_f/2}=\kappa_c\frac{dT_f(z)}{dz}\bigg|_{z=h_f/2}$$

$$\kappa_p\frac{d\widetilde{T}_p(z)}{dz}\bigg|_{z=-h_f/2}=\kappa_m\frac{dT_f(z)}{dz}\bigg|_{z=-h_f/2} \tag{9}$$

The solution of Eq. (5) with the aforementioned conditions can be expressed as polynomial series:

$$T_p(z)=T_1+\frac{T_U-T_1}{h_p}\left(z-h_f/2\right) \tag{10}$$

$$\widetilde{T}_p(z)=T_L+\frac{T_2-T_L}{h_p}\left(z+h_f/2+h_p\right) \tag{11}$$

and

$$T_f(z)=A_0+A_1\left(\frac{z}{h_f}+\frac{1}{2}\right)+A_2\left(\frac{z}{h_f}+\frac{1}{2}\right)^{n+1}+$$

$$A_3\left(\frac{z}{h_f}+\frac{1}{2}\right)^{2n+1}+A_4\left(\frac{z}{h_f}+\frac{1}{2}\right)^{3n+1}+$$

$$A_5\left(\frac{z}{h_f}+\frac{1}{2}\right)^{4n+1}+A_6\left(\frac{z}{h_f}+\frac{1}{2}\right)^{5n+1}+O(z)^{6n+1} \tag{12}$$

where constants T_1, T_2 and A_j can be found in Appendix A.

4. Nonlinear piezo-thermo-electric coupled FG circular plate system

It is assumed that an FGM circular plate is sandwiched between two thin piezoelectric layers which are sensitive in both circumferential and radial directions and the structure is in thermal environment; also, the piezoelectric layers are much thinner than the FGM plate, i.e., $h_p << h_f$. An initial large deformation exceeding the linear range is imposed on the circular plate and a von-Karman type nonlinear deformation is adopted in the analysis. The von-Karman type nonlinearity assumes that the transverse nonlinear deflection w is much more prominent than the other two inplane deflections.

4.1 Nonlinear strain-displacement relations

Based on the Kirchhoff-Love assumptions, the strain components at distance z from the middle plane are given by

$$\varepsilon_{rr}=\overline{\varepsilon}_{rr}+zk_{rr} \, ,$$

$$\varepsilon_{\theta\theta}=\overline{\varepsilon}_{\theta\theta}+zk_{\theta\theta} \, ,$$

$$\varepsilon_{r\theta}=\overline{\varepsilon}_{r\theta}+zk_{r\theta} \tag{13}$$

where the z-axis is assumed positive outward. Here $\overline{\varepsilon}_{rr}$, $\overline{\varepsilon}_{\theta\theta}$, $\overline{\varepsilon}_{r\theta}$ are the engineering strain components in the median surface, and k_{rr}, $k_{\theta\theta}$, $k_{r\theta}$ are the curvatures which can be expressed in terms of the displacement components. The relations between the middle plane strains and the displacement components according to the von-Karman type nonlinear deformation and Sander's assumptions [25] are defined as:

$$\overline{\varepsilon}_{rr}=\frac{\partial u_r}{\partial r}+\frac{1}{2}\left(\frac{\partial w}{\partial r}\right)^2$$

$$\overline{\varepsilon}_{\theta\theta}=\frac{1}{r}\frac{\partial u_\theta}{\partial\theta}+\frac{u_r}{r}+\frac{1}{2}\left(\frac{1}{r}\frac{\partial w}{\partial\theta}\right)^2$$

$$\overline{\varepsilon}_{r\theta}=\frac{1}{r}\frac{\partial u_r}{\partial\theta}+\frac{\partial u_\theta}{\partial r}-\frac{u_\theta}{r}+\left(\frac{1}{r}\frac{\partial w}{\partial r}\right)\frac{\partial w}{\partial\theta} \tag{14}$$

$$\kappa_{rr}=-\frac{\partial^2 w}{\partial r^2}$$

$$\kappa_{\theta\theta} = -\frac{1}{r}\frac{\partial w}{\partial r} - \frac{1}{r^2}\frac{\partial^2 w}{\partial \theta^2}$$

$$\kappa_{r\theta} = -\frac{1}{r}\left(\frac{\partial^2 w}{\partial r\partial\theta}\right) + \frac{1}{2r^2}\frac{\partial w}{\partial\theta} \qquad (15)$$

where u_r, u_θ, w represent the corresponding components of the displacement of a point on the middle plate surface. Substituting Eqs. (14) and (15) into Eqs. (13), the following expressions for the strain components are obtained

$$\varepsilon_{rr} = \frac{\partial u_r}{\partial r} + \frac{1}{2}\left(\frac{\partial w}{\partial r}\right)^2 - z\frac{\partial^2 w}{\partial r^2}$$

$$\varepsilon_{\theta\theta} = \frac{1}{r}\frac{\partial u_\theta}{\partial\theta} + \frac{u_r}{r} + \frac{1}{2}\left(\frac{1}{r}\frac{\partial w}{\partial\theta}\right)^2 - z\left(\frac{1}{r}\frac{\partial w}{\partial r} + \frac{1}{r^2}\frac{\partial^2 w}{\partial\theta^2}\right)$$

$$\varepsilon_{r\theta} = \frac{1}{r}\frac{\partial u_r}{\partial\theta} + \frac{\partial u_\theta}{\partial r} - \frac{u_\theta}{r} + \left(\frac{1}{r}\frac{\partial w}{\partial r}\right)\frac{\partial w}{\partial\theta} + 2z\left(-\frac{1}{r}\left(\frac{\partial^2 w}{\partial r\partial\theta}\right) + \frac{1}{2r^2}\frac{\partial w}{\partial\theta}\right) \qquad (16)$$

For a circular plate with axisymmetric oscillations, the strain expressions are simplified to

$$\varepsilon_{rr} = \frac{\partial u_r}{\partial r} + \frac{1}{2}\left(\frac{\partial w}{\partial r}\right)^2 - z\frac{\partial^2 w}{\partial r^2}$$

$$\varepsilon_{\theta\theta} = \frac{u_r}{r} - \frac{z}{r}\frac{\partial w}{\partial r}$$

$$\varepsilon_z = \gamma_{r\theta} = \gamma_{\theta z} = \gamma_{zr} = 0 \qquad (17)$$

4.2 Force and moment resultants

The stress components in the FG core plate in terms of strains based on the generalized Hooke's Law using the plate theory approximation of $\sigma_z \approx 0$ in the constitutive equations are defined as [26];

$$\sigma_r^f = \frac{E(z)}{1-v^2}(\varepsilon_r + v\varepsilon_\theta) - \frac{E(z)\alpha(z)}{1-v}\Delta T \qquad (18)$$

$$\sigma_\theta^f = \frac{E(z)}{1-v^2}(\varepsilon_\theta + v\varepsilon_r) - \frac{E(z)\alpha(z)}{1-v}\Delta T \qquad (19)$$

where E(z), v(z) and α(z) are Young's modulus, Poisson's ratio and coefficient of thermal expansion of the FGM material, respectively, as expressed in Eq.(4), where $\Delta T = T(z) - T_0$ is temperature rise from the stress-free reference temperature (T_0) which is assumed to exist at a temperature of $T_0 = 0$ and $T(z)$ is presented in Eqs. (10)-(12).

The moments and membrane forces include both mechanical and electric components as

$$N_r = N_r^m - N_r^e - N_r^t, \quad N_\theta = N_\theta^m - N_\theta^e - N_\theta^t, \qquad (20)$$

$$M_r = M_r^m - M_r^e - M_r^t, \quad M_\theta = M_\theta^m - M_\theta^e - M_\theta^t$$

where the superscripts m, e, and t, respectively, denote the mechanical, electric, and temperature components. Mechanical forces and moments of the thin circular plate made of functionally graded material can be expressed as

$$(N_r^m, N_\theta^m) = \int_{-h_f/2}^{h_f/2}(\sigma_{rr}, \sigma_{\theta\theta})dz \qquad (21)$$

$$(M_r^m, M_\theta^m) = \int_{-h_f/2}^{h_f/2}(\sigma_{rr}, \sigma_{\theta\theta})zdz \qquad (22)$$

$$(N_{r\theta}^m, M_{r\theta}^m) = \int_{-h_f/2}^{h_f/2}(1, z)\sigma_{r\theta}dz \qquad (23)$$

Substituting Eqs. (13) and (18), (19) into Eqs. (22)-(23) gives the following constitutive relations for mechanical forces and moments of FG plate :

$$N_r^m = D_1(\bar\varepsilon_{rr} + v\bar\varepsilon_{\theta\theta}),$$

$$N_\theta^m = D_1(\bar\varepsilon_{\theta\theta} + v\bar\varepsilon_{rr}) \qquad (24)$$

$$M_r^m = D_2(\kappa_{rr} + v\kappa_{\theta\theta}),$$

$$M_\theta^m = D_2(\kappa_{\theta\theta} + v\kappa_{rr}) \qquad (25)$$

$$N_r^t = N_\theta^t = \int_{-h_t/2}^{h_t/2}\frac{\alpha(z)E(z)}{1-v}\Delta T(z)\,dz, \qquad (26)$$

$$M_r^t = M_\theta^t = \int_{-h_t/2}^{h_t/2}\frac{\alpha(z)E(z)}{1-v}\Delta T(z)zdz \qquad (27)$$

in which the coefficients of D_1 and D_2 in the above equations are related to the plate stiffness and are given by

$$D_1 = \int_{-h_f/2}^{h_f/2}\frac{E_f(z)}{1-v_f^2}dz \quad , \quad D_2 = \int_{-h_f/2}^{h_f/2}z^2\frac{E_f(z)}{1-v_f^2}dz \qquad (28)$$

It is assumed that the piezoelectric layers are sensitive in both radial and circumferential directions and the piezoelectric permeability constants $e_{31} = e_{32}$. Hence, the electric membrane forces and bending moments are induced by the converse piezoelectric effect on the piezoelectric actuators, and these forces vary linearly across the plate thickness as [27];

$$N_r^e = N_\theta^e = -e_{31}\left(V_z^t + V_z^b\right)/2, \qquad (29)$$

$$M_r^e = M_\theta^e = -e_{31}\left(h_f + h_p\right)\left(V_z^t - V_z^b\right)/2, \qquad (30)$$

in which V_z^t and V_z^b are the control voltages applied to the top and bottom piezoelectric layers, respectively.

4.3 System electromechanical equations

Axisymmetric free oscillation equations of the piezoelectric coupled circular FG plate in thermal environment can be derived from the generic piezoelectric shell equations using four system parameters: two Lame parameters, $A_1 = 1$, $A_2 = r$, where r is the radial distance measured from the center, and two radii, $R_1 = \infty$, $R_2 = \infty$ [28, 29] as

$$\frac{\partial(rN_r)}{\partial r} - N_\theta = 0 \tag{31}$$

$$\frac{1}{r}\frac{\partial(rQ_{rz})}{\partial r} + N_r \frac{\partial^2 w}{\partial r^2} + N_{\theta\theta}\left(\frac{1}{r}\frac{\partial w}{\partial \theta}\right) - I_1 \frac{\partial^2 w}{\partial t^2} = 0 \tag{32}$$

in which $I_1 = \left(\int_{-h_f/2}^{h_f/2} \rho_f(z)dz\right)$ and the transverse shear component Q_{rz} is related to moments as

$$Q_{rz} = \frac{1}{r}\left[\frac{\partial(rM_r)}{\partial r} - M_\theta\right] \tag{33a,b}$$

Note that only the normal radial strain keeps the quadratic nonlinear term. Substituting all force/moment components and strain-displacement equations into the radial and transverse Eqs. (31), (32) yields

$$r\frac{\partial}{\partial r}\left[\frac{1}{r}\frac{\partial}{\partial r}\left(r^2 N_r^m\right)\right] = -\frac{Y}{2}\left(\frac{\partial w}{\partial r}\right)^2 \tag{34}$$
$$+ \frac{\partial}{\partial r}\left[r^2 \frac{\partial}{\partial r}\left(N_r^e + N_r^t\right)\right] + \nu\, r\frac{\partial}{\partial r}\left(N_r^e + N_r^t\right)$$

$$\frac{D_2}{r}\frac{\partial}{\partial r}\left(r\frac{\partial}{\partial r}\left[\frac{1}{r}\frac{\partial}{\partial r}\left(r\frac{\partial}{\partial r}w(r,t)\right)\right]\right) = -I_1\frac{\partial^2 w}{\partial t^2} \tag{35}$$
$$+ \frac{1}{r}\frac{\partial}{\partial r}\left[r\frac{\partial w}{\partial r}\left(N_r^m - N_r^e - N_r^t\right)\right] - \frac{1}{r}\frac{\partial}{\partial r}\left[r\frac{\partial}{\partial r}\left(M_r^e + M_r^t\right)\right]$$

in which $Y = \left(\int_{-h_f/2}^{h_f/2} E_f(z)dz\right)$ and boundary conditions at the center of the plate with axisymmetric oscillations are defined as

(1) Plate center (r=0):

Slope: $\dfrac{\partial w}{\partial r} = 0$

Radial force: N_{rr}^m : finite $\tag{36a,b}$

Boundary conditions for the simply supported (immovable) circumference are defined as:

(2) Plate circumference   (r=a):

(i) $w = 0$ $\tag{37a}$

(ii) $\dfrac{\partial}{\partial r}(rN_r^m) - \nu N_r^m = r\dfrac{\partial}{\partial r}(N_r^e + N_r^t)$ $\tag{37b}$

(iii) $-D_2\left(\dfrac{\partial^2 w}{\partial r^2} + \dfrac{\nu}{r}\dfrac{\partial w}{\partial r}\right) = (M_r^e + M_r^t)$ $\tag{37c}$

It is further assumed that the control potentials on the top and bottom piezoelectric actuators are of equal magnitudes and opposite signs, i.e., $V_z^t = -V_z^b = \hat{V}$ and the plate is subjected to a uniform temperature excitation of $T(z)$. Accordingly, the electric and temperature induced forces and moments can be defined as:

$$N_r^e = N_\theta^e = 0 \tag{38a}$$

$$M_r^e = M_\theta^e = M^e = -e_{31}\left(h_f + h_p\right)\hat{V}, \tag{38b}$$

$$N_\theta^t = N_r^t = N^t, \tag{39a}$$

$$M_\theta^t = M_r^t = M^t, \tag{39b}$$

Using these force and moment expressions, one can further simplify the open-loop plate equations and boundary conditions:

$$r\frac{\partial}{\partial r}\left[\frac{1}{r}\frac{\partial}{\partial r}\left(r^2 N_r^m\right)\right] = -\frac{Y}{2}\left(\frac{\partial w}{\partial r}\right)^2 \tag{40}$$

$$\frac{D_2}{r}\frac{\partial}{\partial r}\left(r\frac{\partial}{\partial r}\left[\frac{1}{r}\frac{\partial}{\partial r}\left(r\frac{\partial}{\partial r}w(r,t)\right)\right]\right) = $$
$$-I_1\frac{\partial^2 w}{\partial t^2} + \frac{1}{r}\frac{\partial}{\partial r}\left[r\frac{\partial w}{\partial r}\left(N_r^m - N^t\right)\right] \tag{41}$$

Boundary conditions become

(1) Plate center (r=0):

Slope: $\dfrac{\partial w}{\partial r}\bigg|_{r=0}$

Radial force: $N_r^m\big|_{r=0}$ *: finite* $\tag{42a,b}$

(2) Plate circumference   (r=a):

(i) $w\big|_{r=a} = 0$ $\tag{43a}$

(ii) $\left[\dfrac{\partial}{\partial r}(rN_r^m) - \nu N_r^m\right]_{r=a} = 0$ $\tag{43b}$

(iii) $\left[-D_2\left(\dfrac{\partial^2 w}{\partial r^2} + \dfrac{\nu}{r}\dfrac{\partial w}{\partial r}\right)\right]_{r=a} = (M^e + M^t)$ $\tag{43c}$

4.4 Simplification and normalization

Solutions of the transverse displacement w and radial force N_r^m of the above open-loop plate equations and boundary conditions can be expressed as a summation of a static component and a dynamic component as

$$w(r,t) = w_s(r) + w_d(r,t),$$
$$N_r^m(r,t) = N_{r_s}^m(r,t) + N_{r_d}^m(r,t) \tag{44a,b}$$

where $w_s(r)$ and $N_{r_s}^m(r,t)$ are the static solutions, $w_d(r,t)$ and $N_{r_d}^m(r,t)$ are the dynamic solutions, and the subscripts *s* and *d,* respectively, denote the static and dynamic solutions.

Accordingly, the solution procedure can be divided into two parts. The first part deals with the nonlinear static solutions, and the second part deals with the dynamic solutions. In addition, normalized dimensionless quantities are adopted in the static and dynamic analyses. These dimensionless quantities are defined by known geometrical and material parameters [30]:

radial distance: $y = (r/a)^2$,

transverse deflection: $\overline{w}_s = \sqrt{3(1-v^2)}\dfrac{w_s}{h_f}$,

slope: $X_s(y) = y\dfrac{dw_s}{dy}$,

static force: $Y_s^m(y) = \left(a^2 N_{r_s}^m / 4D_2\right)y$

temperature load: $T* = \left(a^2 N^t / 4D_2\right)$

radial distance: $x = (r/a)$,

dynamic deflection: $\overline{w}_d = \sqrt{3(1-v^2)}\dfrac{w_d}{h_f}$,

dynamic force: $Y_d^m(y) = \left(a^2 N_{r_d}^m / D_2\right)$

voltage: $V = \left[3(1-v^2)\right]^{1/2} e_{31}(h_f + h_p)\hat{V} / \left(2D_2 h_f\right)$

Substituting these normalized dimensionless quantities into the open-loop plate equations and boundary conditions of axisymmetric plate oscillations and separating the static parts from the dynamic parts gives the static equations and dynamic equations with their associated boundary conditions:

(1) Static Equations and Boundary Conditions

$$y^2 \frac{d^2 X_s}{dy^2} = X_s Y_s^m - T * y X_s ,\tag{45}$$

$$y^2 \frac{d^2 Y_s^m}{dy^2} = -\frac{1}{2}(X_s)^2 , \qquad 0 < y < 1\tag{46}$$

Boundary conditions at center y = 0:

(i) $X_s\big|_{y=0} = 0$, (ii) $Y_s^m\big|_{y=0} = 0$ (47a,b)

Boundary conditions on circumference y = 1:

(i) $\left[(1+v)Y_s^m - 2\dfrac{dY_s^m}{dy}\right]_{y=1} = 0$,

(ii) $\left[(1-v)\dfrac{X_s}{y} - 2\dfrac{dX_s^m}{dy}\right]_{y=1} = V\big|_{y=1}$ (48a,b)

(2) Dynamic Equations and Boundary Conditions

$$x\frac{\partial}{\partial x}\left(\frac{1}{x}\frac{\partial}{\partial x}\left[x^2 Y_d^m\right]\right) = -2\left[\frac{d\overline{w}_s}{dx}\frac{\partial\overline{w}_d}{\partial x} - \frac{1}{2}\left(\frac{\partial\overline{w}_d}{\partial x}\right)^2\right]\tag{49}$$

$$\frac{1}{x}\frac{\partial}{\partial x}\left\{x\frac{\partial}{\partial x}\left[\frac{1}{x}\frac{\partial}{\partial x}\left(x\frac{\partial}{\partial x}(\overline{w}_d)\right)\right]\right\} = -\frac{I_1 a^4}{D_2}\frac{\partial^2\overline{w}_d}{\partial t^2}$$

$$+\frac{1}{x}\frac{\partial}{\partial x}\left[xY_d^m\frac{d\overline{w}_s}{dx} + \frac{4}{x}Y_s^m\frac{\partial\overline{w}_d}{\partial x} + xY_d^m\frac{\partial\overline{w}_d}{\partial x}\right]-\tag{50}$$

$$4\hat{T}\frac{1}{x}\frac{\partial}{\partial x}\left(x\frac{\partial\overline{w}_d}{\partial x}\right)$$

Boundary conditions at center *x* = 0:

(i) $\dfrac{\partial\overline{w}_d}{\partial x}\bigg|_{x=0} = 0$, (ii) $Y_d^m\big|_{x=0} = finite$ (51a,b)

Boundary conditions on circumference *x* = 1:

(i) $\overline{w}_d\big|_{x=1} = 0$,

(ii) $\left[v\dfrac{\partial}{\partial x}(Y_d^m) + (1-v)Y_d^m\right]_{x=1} = 0$

(iii) $\left[\dfrac{\partial^2\overline{w}_d}{\partial x^2} + v\dfrac{\partial\overline{w}_d}{\partial x}\right]_{x=1} = 0$, (52a,b,c)

5. Static solutions

For the nonlinear static equations and boundary conditions of the boundary value problem derived above, static solutions of slopes $X_s(y)$ and forces $Y_s^m(y)$ can be represented in (exact) series expansion forms [30]:

$$X_s(y) = \sum_{i=1}^{\infty} A_i y^i , \quad Y_s^m(y) = \sum_{i=1}^{\infty} B_i y^i \quad 0 \le y \le 1\tag{53a,b}$$

where A_i and B_i are constant coefficients. Substituting the series solutions, Eqs. (53a & b), into static equations, Eqs. (45) & (46), and grouping coefficients of y^i one can obtain the recurrence equations for coefficients A_i and B_i:

$$A_i = \frac{1}{i(i-1)}\sum_{j=1}^{i-1} A_j B_{i-j} - \hat{T}A_{i-1} ,$$

$$B_i = \frac{-1}{2i(i-1)}\sum_{j=1}^{i-1} A_j A_{i-j} , \qquad i = 2,3,4,...\tag{54a,b}$$

It is observed that only A_1 and B_1 are independent constants, and the others are dependent. As long as A_1 and B_1 are determined by the boundary conditions, other coefficients A_i and B_i can be calculated from the recurrence equations. Accordingly, static series solutions are completed. The series solutions of $Y_s^m(y)$ and $X_s(y)$ satisfy the boundary conditions at y = 0, Eqs. (47a,b). Substituting the assumed series solutions $Y_s^m(y)$ and $X_s(y)$ into the boundary conditions at y = 1, Eqs. (48a,b), yields

$$\sum_{i=1}^{\infty}\left[(1+v-2i)B_i\right] = 0 , \quad \sum_{i=1}^{\infty}\left[(1-v-2i)A_i\right] = V\tag{55a,b}$$

A_i and B_i can be determined from the nonlinear algebraic equations Eqs. (55a,b) using the Newton-Raphson iteration method [31]. Define

$$\alpha(A_1, B_1) = \sum_{i=1}^{\infty}\left[(1-v-2i)A_i\right] - V ,$$

$$\beta(A_1, B_1) = \sum_{i=1}^{\infty}\left[(1+v-2i)B_i\right]\tag{56a,b}$$

$$\overline{A}_1 = A_1 + \Delta_1, \quad \overline{B}_1 = B_1 + \Delta_2 \tag{57a,b}$$

in which

$$\Delta_1 =$$
$$\frac{1}{\Delta}\left[\beta(A_1,B_1)\frac{\partial}{\partial B_1}\alpha(A_1,B_1) - \alpha(A_1,B_1)\frac{\partial}{\partial B_1}\beta(A_1,B_1)\right]$$

$$\Delta_2 =$$
$$\frac{1}{\Delta}\left[\alpha(A_1,B_1)\frac{\partial}{\partial A_1}\beta(A_1,B_1) - \beta(A_1,B_1)\frac{\partial}{\partial A_1}\alpha(A_1,B_1)\right] \tag{58a,b}$$

and

$$\Delta = \det\begin{bmatrix} \dfrac{\partial}{\partial A_1}\alpha(A_1,B_1) & \dfrac{\partial}{\partial B_1}\alpha(A_1,B_1) \\[2mm] \dfrac{\partial}{\partial A_1}\beta(A_1,B_1) & \dfrac{\partial}{\partial B_1}\beta(A_1,B_1) \end{bmatrix} \neq 0 \tag{58c}$$

$\overline{A}_1$ and $\overline{B}_1$ are, respectively, the iteration values of A_1 and B_1; Δ_1 and Δ_2 are the correction factors of A_1 and B_1 at each iteration. The partial derivatives $\partial\alpha/\partial A_1$, $\partial\alpha/\partial B_1$, $\partial\beta/\partial A_1$ and $\partial\beta/\partial B_1$, can be determined from the definitions of $\alpha(A_1,B_1)$ and $\beta(A_1,B_1)$. These iterations are repeated until they reach their prescribed limits, say $|\alpha|$, $|\beta|$, $|\Delta_1|$ and $|\Delta_2|$ are smaller than 10^{-4}. Accordingly, a set of A_1 and B_1 are determined for a set of given control voltages V and temperatures $\hat{T}$. Using the recurrence equations, one can determine all other $A_i's$ and $B_i's$, and further the nonlinear static solutions of slope $X_s(y)$ and static force $Y_s^m(y)$. Knowing the slope, one can determine the static deflections $\overline{w}_s$ and w_s of the nonlinear circular plate subject to voltage and temperature excitations.

6. Dynamic solutions

It is assumed that the FG circular plate is oscillating in the vicinity of the nonlinearly deformed static equilibrium position. FG index, voltage and temperature effects to the natural frequencies and amplitude/frequency relations are investigated in this section. First, linearized eigenvalue equations are solved using the exact series solutions. Then nonlinear amplitude and frequency relations of nonlinear large amplitude free vibrations are investigated using the Galerkin method and the perturbation method.

6.1 Eigenvalue equations

Neglect the nonlinear terms in the normalized dynamic equations, and then assume following harmonic solutions of displacement and dynamic force

$$\overline{w}_d(x,t) = R_d(x)\sin(\omega_n t) \tag{59a}$$

$$Y_d^m(x,t) = S_d(x)\sin(\omega_n t) \tag{59b}$$

where ω_n is the natural frequency; $R_d(x)$ and $S_d(x)$ are

the (linear) eigenfunctions or mode shape functions of $\overline{w}_d(x,t)$ and $Y_d^m(x,t)$, respectively. $R_d(x)$ defines the mode shape function, and $S_d(x)$ defines the spatial force distribution. Both $R_d(x)$ and $S_d(x)$ have to satisfy the boundary conditions, and they are also assumed in the series expansion forms. Substituting Eqs. (59a, b) into the dynamic equations and boundary conditions, Eqs. (49)-(52), yields

$$x\frac{d}{dx}\left(\frac{1}{x}\frac{d}{dx}\left[x^2 S_d(x)\right]\right) = -2\frac{d\overline{w}_s}{dx}\frac{dR_d}{dx} \tag{60}$$

$$\frac{1}{x}\frac{d}{dx}\left\{x\frac{d}{dx}\left[\frac{1}{x}\frac{d}{dx}\left(x\frac{d}{dx}(R_d(x))\right)\right]\right\} =$$
$$\lambda R_d(x) + \frac{1}{x}\frac{d}{dx}\left[2xS_d(x)\frac{d\overline{w}_s}{dx} + \frac{4}{x}Y_s^m\frac{dR_d}{dx}\right] \tag{61}$$
$$-4\hat{T}\frac{1}{x}\frac{d}{dx}\left[x\frac{dR_d}{dx}\right] \qquad ,0 < x < 1$$

where λ is the eigenvalue and $\lambda = I_1\dfrac{a^4}{D_2}\omega_n^2$. Boundary conditions become

Center x=0:

$$\left.\frac{dR_d}{dx}\right|_{x=0} = 0, \quad \left.S_d(x)\right|_{x=0} : \text{finite} \tag{62a,b}$$

Circumference x=1:

$$\left.R_d\right|_{x=1} = 0,$$
$$\left[\nu\frac{d}{dx}[S_d(x)] + (1-\nu)S_d(x)\right]_{x=1} = 0,$$
$$\left[\frac{d^2 R_d}{dx^2} + \nu\frac{dR_d}{dx}\right]_{x=1} = 0 \tag{63a,b,c}$$

Again, assume the eigenfunctions take the series expansion forms:

$$R_d(x) = \sum_{i=0}^{\infty} a_i x^{2i}, \quad S_d(x) = \sum_{i=0}^{\infty} b_i x^{2i} \tag{64a,b}$$

where a_i and b_i, are constants determined by eigenvalue equations and boundary conditions. The series solutions $R_d(x)$ and $S_d(x)$ satisfy the boundary conditions at x = 0, Eqs. (62a,b). Assume a_i and b_i, be represented by the linear combinations of independent constants a_0, a_1 and b_0.

$$a_i = f_{i1}a_0 + f_{i2}a_1 + f_{i3}b_0, \tag{65a}$$
$$b_i = g_{i1}a_0 + g_{i2}a_1 + g_{i3}b_0, \quad i=1,2,3,... \tag{65b}$$

where f_{ij} and g_{ij} are to be determined. Substituting the series expressions of modes $R_d(x)$ and forces $S_d(x)$ into the dynamic equations, one can derive a set of recurrence equations of a_i and b_i. Then, using expressions of a_i and b_i of Eqs. (65a, b), one can further determine the coefficients f_{ij} and g_{ij}

$$f_{01} = 1, \quad f_{02} = f_{03} = 0;$$

$f_{11} = 0, \quad f_{12} = 1, \quad f_{13} = 0;$

$g_{01} = 0, \quad g_{02} = 0, \quad g_{03} = 1;$

$g_{ik} = -\dfrac{2}{i(i+1)} \displaystyle\sum_{j=1}^{i} jf_{jk} A_{i-j+1}, i = 1,2,3,\dots, \quad k = 1,2,3.$

$f_{21} = \lambda/64, \quad f_{22} = (B_1 - T^*)/4, \quad f_{23} = A_1/8,$

$f_{31} = [A_1 g_{11} + 4f_{21}(B_1 - T^*)]/36,$

$f_{32} = \{\lambda + 32B_2 + 16[A_1 g_{12} + 4f_{22}(B_1 - T^*)]\}/24,$

$f_{33} = [A_1 g_{13} + 4f_{23}(B_1 - T^*) + A_2]/36,$

$f_{(i+2)k} = \Big[\lambda f_{ik} - 16T^*(i+1)^2 + 8(i+1) \times$

$\displaystyle\sum_{j=1}^{i+1}\big(2jf_{ik}B_{i-k+2} + A_j g_{(i-j+1)k}\big)\Big][4(i+1)(i+2)]^{-2}$

$i = 2,3,4,\dots, \quad \text{and} \quad k = 1,2,3.$

Substituting these coefficients into the boundary conditions at $x = 1$, one can obtain an explicit matrix representation of the eigenvalue equation.

$$\begin{bmatrix} h_{11} & h_{12} & h_{13} \\ h_{21} & h_{22} & h_{23} \\ h_{31} & h_{32} & h_{33} \end{bmatrix} \begin{bmatrix} a_0 \\ a_1 \\ b_0 \end{bmatrix} = [0] \tag{66}$$

where h_{ij} are defined by

$$h_{1k} = \sum_{i=0i1}^{\infty} f_{ik}, \quad k = 1,2,3. \tag{67a}$$

$$h_{2k} = \sum_{i=0}^{\infty} [iv + i(2i-1)]f_{ik}, \quad k = 1,2,3. \tag{67b}$$

$$h_{3k} = \sum_{i=0}^{\infty} [2iv + (1-v)]g_{ik}, \quad k = 1,2,3. \tag{67c}$$

These h_{ik} coefficients are functions of eigenvalues λ, and accordingly, the determinant of the coefficient matrix leads to a nonlinear characteristic equation. Using the Newton-Raphson iteration method [31], one can calculate eigenvalues and furthermore natural frequencies and mode shape functions of the nonlinear FG circular plate.

6.2 Nonlinear large amplitude free vibrations

In this section, the perturbation method is used to investigate the nonlinear large amplitude effect to natural frequencies of the piezoelectric laminated FG circular plate. Assume an approximate solution of the nonlinear response $\overline{w}_d(x,t)$ be a product of a spatial function $\overline{w}_d^*(x)$ and a temporal function $f(t)$;

$$\overline{w}_d(x,t) = \overline{w}_d^*(x)f(t), \tag{68}$$

where $\overline{w}_d^*(x)$ is a test function satisfying the boundary conditions:

Plate center x=0: $\left.\dfrac{\partial \overline{w}_d^*}{\partial x}\right|_{x=0} = 0,$ (69a)

Plate circumference x=1:

$\left.\overline{w}_d^*\right|_{x=1} = 0, \quad \left[\dfrac{\partial^2 \overline{w}_d^*}{\partial x^2} + v\dfrac{\partial \overline{w}_d^*}{\partial x}\right]_{x=1} = 0$ (69b,c)

Substituting Eq. (68) into the dynamic equation Eq. (49) and using the Galerkin method, one can derive a nonlinear equation for $f(\tau)$

$$f_{,\tau\tau} + f(\tau) + \mu_1 f^2(\tau) + \mu_2 f^3(\tau) = 0, \tag{70}$$

where $\tau = \omega t$ and μ_1 and μ_2 are the nonlinear coefficient functions, ω is defined by

$$\omega^2 = (c_1 + c_3)/c_2., \tag{71}$$

c_1, c_2 and c_3 are defined by integrals:

$$c_1 = \int_0^1 \left\{\overline{w}_d^*(x)\frac{d}{dx}\left\{x\frac{d}{dx}\left[\frac{1}{x}\frac{d}{dx}\left(x\frac{d}{dx}(\overline{w}_d^*(x))\right)\right]\right\}\right\}dx \tag{72a}$$

$$c_2 = \int_0^2 \left(\overline{w}_d^*(x)\right)^2 x\,dx \tag{72b}$$

$c_3 =$

$$-\int_0^1 \overline{w}_d^*(x)\frac{d}{dx}\left[\frac{4}{x}Y_s^m\frac{d\overline{w}_d^*}{dx} + 2xN_{r_d}^{*l}\frac{d\overline{w}_s}{dx} - 4T^*x\frac{d\overline{w}_d^*}{dx}\right]dx \tag{72c}$$

in which $N_{r_d}^{*l}(x)$ and $N_{r_d}^{*n}(x)$ are the linear and nonlinear force components. The nonlinear coefficient functions μ_1 and μ_1 are defined by

$$\mu_1 = c_4/(c_1 + c_3), \quad \mu_2 = c_5/(c_1 + c_3) \tag{73a,b}$$

where c_4 and c_5 are defined by integrals:

$$c_4 = -\int_0^1 \overline{w}_d^*(x)\frac{d}{dx}\left[2xN_{r_d}^{*n}(x)\frac{d\overline{w}_s(x)}{dx} + N_{r_d}^{*l}(x)\frac{d\overline{w}_d^*(x)}{dx}\right]dx \tag{74a}$$

$$c_5 = -\int_0^1 \overline{w}_d^*(x)\frac{d}{dx}\left[xN_{r_d}^{*n}(x)\frac{d\overline{w}_d^*(x)}{dx}\right]dx \tag{74b}$$

The linear and nonlinear force components are written as

$$N_{r_d}^{*l}(x) = \frac{1}{x^2}\int_0^1 G(x,\xi)\frac{1}{\xi}\frac{dw_s}{d\xi}\frac{d\overline{w}_d^*}{d\xi}\,d\xi \tag{75a}$$

$$\overline{N}_{r_d}^{*n}(x) = \frac{1}{4x^2}\int_0^1 G(x,\xi)\frac{1}{\xi}\left(\frac{d\overline{w}_d^*}{d\xi}\right)^2 d\xi \tag{75b}$$

The kernel function

$$G(x,\xi) = \begin{cases} \left[1 - ((1+v)/(1-v))\xi^2\right]x^2 & x < \xi, \\ \left[1 - ((1+v)/(1-v))x^2\right]\xi^2 & x \geq \xi, \end{cases} \tag{76}$$

Since the mode shape functions of the linear free vibrations were determined previously, it is convenient to select the mode shape functions as the trial functions,

$$\overline{w}_d^*(x) = R_d(x), \tag{77a}$$

$$N_{r_d}^{*l}(x) = S_d(x), \quad 0 \le x \le 1; \tag{77b}$$

Table 1. Material properties [13].

Material	Property					
	E (GPa)	ρ (kg/m³)	v	α (1/℃)	κ (W/mK)	d_{31}, d_{32} (m/V)
Aluminum	70	2707	0.3	23e-6	204	-
Alumina	380	3800	0.3	7.4e-6	10.4	-
PZT	63	7600	0.3	1.2e-4	0.17	1.79e-10

and the frequency can be selected as the natural frequencies determined previously. Using the Krylov-Bogoliubov-Mitropolsky perturbation method [32] and solving the nonlinear dynamic equation Eq. (70), one can obtain the amplitude-frequency relation as

$$p = \frac{\omega}{\omega_n} = 1 + \frac{1}{24}\left(9\mu_2 - 10\mu_1^2\right)\hat{a}^2 + \frac{5}{8}\mu_1\mu_2\hat{a}^3 + ... \tag{78}$$

where ω is the (nonlinear vibration) frequency; ω_n is the natural frequency; $\hat{a}$ is the dimensionless vibration amplitude; and μ_1 and μ_2 are the nonlinear coefficient functions. Note that the ratio is unity, i.e., $p = \omega/\omega_n = 1$, if the system is linear. Once the coefficients μ_1 and μ_2 are calculated, one can further evaluate the amplitude and frequency relations of

Table 2. Values of the normalized dimensionless center deflections with respect to the normalized dimensionless piezoelectric voltages for various normalized temperatures computed by two methods (present series solution and FEM) (v=0.3, n=1000).

Normalized Voltage (V)	Normalized Temperature($T*$)								
	$T* = -0.2$			$T* = -0.1$			$T* = 0$		
	Present	FEM	Diff. (%)	Present	FEM	Diff. (%)	Present	FEM	Diff. (%)
0	0	0	0	0	0	0	0	0	0
0.2	0.1239	0.1239	0.038	0.1572	0.1573	0.035	0.1920	0.1921	0.033
0.4	0.2417	0.2418	0.044	0.2984	0.2985	0.043	0.3537	0.3538	0.041
0.6	0.3486	0.3488	0.045	0.4204	0.4206	0.044	0.4875	0.4877	0.042
0.8	0.4427	0.4429	0.052	0.5235	0.5238	0.050	0.5982	0.5985	0.048
1	0.5241	0.5244	0.061	0.6102	0.6106	0.059	0.6904	0.6908	0.051
1.2	0.5942	0.5946	0.059	0.6839	0.6843	0.057	0.7681	0.7685	0.055
1.4	0.6549	0.6553	0.058	0.748	0.7485	0.061	0.8343	0.8348	0.055
1.6	0.7086	0.7091	0.064	0.8056	0.8061	0.059	0.8925	0.8930	0.057
1.8	0.7571	0.7576	0.072	0.8588	0.8594	0.070	0.9447	0.9453	0.059
2	0.802	0.8026	0.069	0.9088	0.9094	0.067	0.9924	0.9930	0.065
2.2	0.8443	0.8449	0.074	0.9561	0.9568	0.069	1.0366	1.0373	0.067
2.4	0.8843	0.8849	0.073	1.0009	1.0016	0.071	1.0777	1.0784	0.068
2.6	0.9216	0.9223	0.074	1.0438	1.0446	0.072	1.1159	1.1167	0.069
2.8	0.9556	0.9563	0.076	1.0865	1.0873	0.074	1.1509	1.1517	0.071
3	0.9855	0.9863	0.079	1.1334	1.1343	0.075	1.1827	1.1836	0.073
	$T* = 0.2$			$T* = 0.5$			$T* = 0.8$		
	Present	FEM	Diff. (%)	Present	FEM	Diff. (%)	Present	FEM	Diff. (%)
0	0	0	0	0	0	0	0	0	0
0.2	0.2736	0.2737	0.034	0.4064	0.4066	0.035	0.5718	0.5720	0.036
0.4	0.4788	0.4790	0.042	0.6633	0.6636	0.043	0.8659	0.8663	0.044
0.6	0.6344	0.6347	0.043	0.8337	0.8341	0.044	1.0272	1.0277	0.045
0.8	0.7550	0.7553	0.044	0.9569	0.9573	0.045	1.1347	1.1352	0.046
1.0	0.8513	0.8517	0.053	1.0547	1.0553	0.054	1.2257	1.2264	0.055
1.2	0.9310	0.9315	0.057	1.1380	1.1387	0.058	1.3118	1.3126	0.060
1.4	0.9993	0.9998	0.057	1.2109	1.2116	0.058	1.3917	1.3925	0.060
1.6	1.0596	1.0603	0.059	1.2746	1.2754	0.060	1.4601	1.4610	0.062
1.8	1.1142	1.1148	0.061	1.3296	1.3304	0.062	1.5147	1.5156	0.064
2.0	1.1640	1.1648	0.067	1.3776	1.3785	0.068	1.5581	1.5592	0.070
2.2	1.2097	1.2106	0.069	1.4214	1.4224	0.070	1.5985	1.5997	0.072
2.4	1.2517	1.2526	0.071	1.4643	1.4653	0.072	1.6458	1.6470	0.074
2.6	1.2902	1.2911	0.072	1.5083	1.5094	0.073	1.7047	1.7060	0.075
2.8	1.3254	1.3264	0.072	1.5510	1.5522	0.075	1.7653	1.7666	0.076
3	1.3581	1.3591	0.072	1.5819	1.5831	0.077	1.7895	1.7909	0.076

the nonlinear circular plate subjected to temperature excitations and control voltages.

7. Results and discussions

Temperature effects of nonlinear static deformations, control voltages, and linear and nonlinear free vibrations of a simply supported piezoelectric laminated functionally graded circular plate are investigated in this section.

7.1 Comparison studies

To ensure the accuracy of the present analysis, an illustrative example is solved. The relevant material properties are listed in Table 1. Since there are no appropriate comparison results available for the problems being analyzed in this paper, we decided to verify the validity of the obtained results by comparing with those of the FEM results. Our FEM model for piezo-FG plate consists of a 3D 8-noded solid element with number of total nodes 26950, number of total elements 24276, 4 DOF per node (3 translation, temperature) in the host plate element and 6 DOF per node (3 translation, temperature, voltage and magnetic properties) in the piezoelectric element. The finite element model has been programmed by the authors, while the standard bilinear interpolations have been employed in finite element approximations.

Table 2 compares the present results of normalized dimensionless central deflections $W_s = \sqrt{3(1-v^2)}\left(w_s/h_f\right)$ with finite element solutions in analyzing the effect of normalized dimensionless piezoelectric voltages $V = \left[3(1-v^2)\right]^{1/2} e_{31}(h_f + h_p)V^*/\left(2D_2 h_f\right)$ to the normalized dimensionless center deflections at various normalized temperatures ($T^* = \left(a^2 N^t/4D_2\right)$) in which a nonlinear deflection-voltage relationship can be observed. As seen from Table 2 the maximum estimated difference of the proposed solution with finite element method is about 0.079%, and a close correlation between these results validates the proposed method of solution.
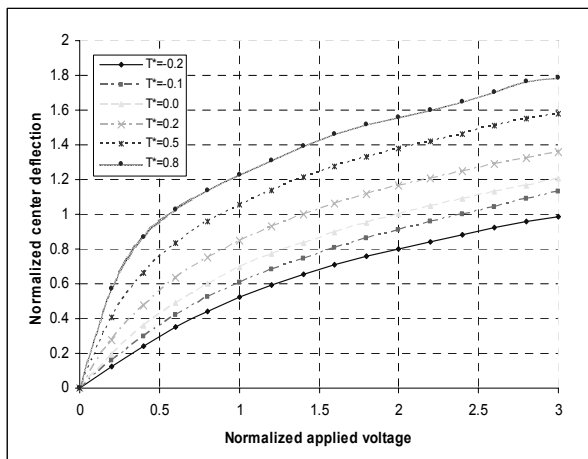
In general, a higher temperature induces higher deflections of the plate, and the deflection at each temperature is attenuated when the control voltage increases and the effect of imposed voltage on the center deflection is nonlinear and this effect is predominant in lesser voltage amounts. This effect can also be seen in the case of considering the temperature environment effect. For example, when $T^* = 0.2$ by increasing the imposed voltage from 0.6 to 1.2 (100%) the normalized dimensionless center deflections increases about 46.8%, while it increases about 34.5% when the imposed voltage increases from 1.2 to 2.4 (100%). In the case of $T^* = 0.5$ by increasing the imposed voltage from 0.6 to 1.2 (100%) the normalized dimensionless center deflection increases about 36.5% while it increases about 28.7% when the imposed voltage increases from 1.2 to 2.4 (100%).

7.2 Parametric studies

Having validated the foregoing formulations, we began to study the large amplitude vibration behavior of FG laminated circular plate subjected to thermo-electro-mechanical loading.
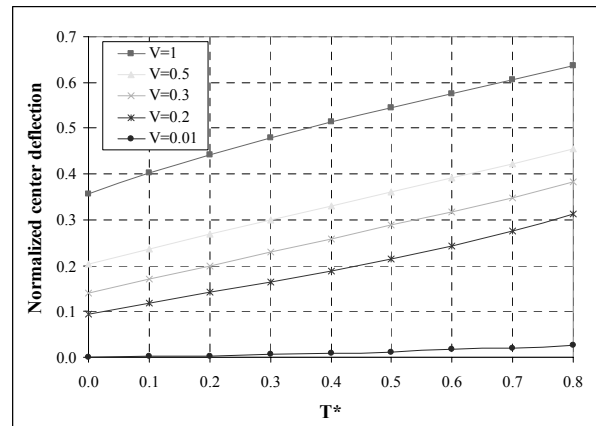

Fig. 2. Normalized Temperature effects to the center deflection for various values of Voltages (n=0.5).

Fig. 1. Effect of applied voltage to the normalized center deflection for various normalized temperatures $T^* = \left(a^2 N^t/4D_2\right)$ (Metal plate).
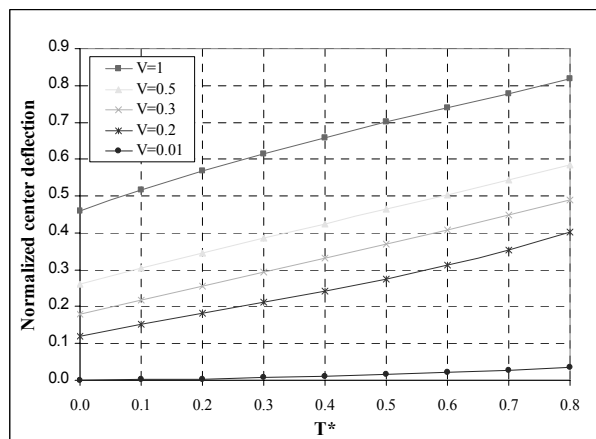

Fig. 3. Normalized Temperature effects to the center deflection for various values of Voltages (n=10).

the results for laminated plates with isotropic substrate layers (that is, the substrate is purely metallic or purely ceramic) and with graded substrate layers (various *n*) are given in both tabular and graphical forms.

To investigate the effect of the applied actuator voltage on the non-linear thermo-electromechanical vibration, the nonlinear normalized center deflection of various graded plates (n = 0.0.1, 0.5, 1, 10, 1000) under various applied normalized voltages (V= 0, 0.2, 0.3, 0.5, 1) is tabulated in Table 3.

Also, the Figs. 4-10 show the effects of the applied actuator voltage, FGM gradient index and normalized temperature on nonlinear normalized center deflection of a piezoelectric coupled circular FGM plate in detail.

It can be noted from the figures that by adjusting the actuator voltage, one can control the shape as well as the deflection of the FGM plate. Also, it is obvious that by increasing the FGM gradient index the normalized center deflection will increase in a nonlinear manner.

For instance, Fig. 2 and Fig. 3 depict the normalized temperature and voltage effects on the center deflection of two graded plates (n=0.5, n=10). It shows that increasing the normalized temperature makes the center deflection increase in various voltages, but this effect is predominant at higher voltages.

Also, in Fig. 4 and Fig. 5 we examine the effect of the temperature gradient on the non-linear thermo-electro-mechanical behavior (center deflection) of FGM plates under two imposed normalized voltages (V= 0, 0.2).

Table 3. FGM index and normalized voltage effects to the nonlinear center deflection.

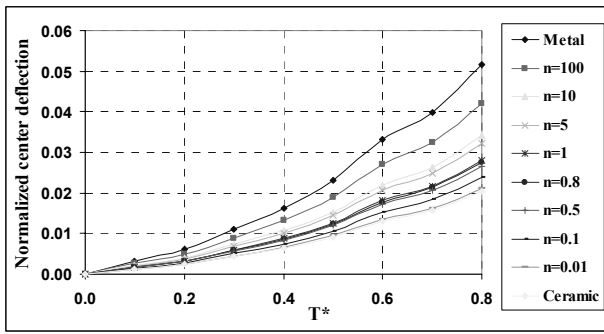| Normalized Temp. (T^*)	FGM index (n) / Normalized Voltage (V)										
	Metal						n=10				
	V=0	V=0.2	V=0.3	V=0.5	V=1		V=0	V=0.2	V=0.3	V=0.5	V=1
0.0	0.0000	0.1820	0.2724	0.3924	0.6925		0.0000	0.1206	0.1805	0.2601	0.4590
0.1	0.0032	0.2288	0.3298	0.4582	0.7790		0.0022	0.1516	0.2186	0.3036	0.5163
0.2	0.0060	0.2738	0.3869	0.5213	0.8573		0.0040	0.1815	0.2564	0.3455	0.5681
0.3	0.0110	0.3188	0.4438	0.5824	0.9288		0.0073	0.2113	0.2941	0.3860	0.6155
0.4	0.0162	0.3654	0.5010	0.6421	0.9949		0.0108	0.2422	0.3320	0.4255	0.6593
0.5	0.0232	0.4155	0.5586	0.7009	1.0569		0.0154	0.2754	0.3702	0.4645	0.7005
0.6	0.0332	0.4706	0.6169	0.7596	1.1164		0.0220	0.3119	0.4089	0.5034	0.7399
0.7	0.0398	0.5326	0.6763	0.8187	1.1745		0.0264	0.3530	0.4482	0.5426	0.7784
0.8	0.0516	0.6071	0.7400	0.8808	1.2329		0.0342	0.4024	0.4905	0.5838	0.8171
(T^*)	n=1						n=0.5				
	V=0	V=0.2	V=0.3	V=0.5	V=1		V=0	V=0.2	V=0.3	V=0.5	V=1
0.0	0.0000	0.0992	0.1484	0.2138	0.3773		0.0000	0.0939	0.1405	0.2024	0.3572
0.1	0.0018	0.1247	0.1797	0.2496	0.4244		0.0017	0.1180	0.1702	0.2364	0.4019
0.2	0.0033	0.1492	0.2108	0.2840	0.4670		0.0031	0.1413	0.1996	0.2689	0.4422
0.3	0.0060	0.1737	0.2418	0.3173	0.5060		0.0057	0.1645	0.2290	0.3004	0.4791
0.4	0.0088	0.1991	0.2729	0.3498	0.5420		0.0084	0.1885	0.2584	0.3312	0.5132
0.5	0.0126	0.2263	0.3043	0.3819	0.5758		0.0120	0.2143	0.2881	0.3616	0.5452
0.6	0.0181	0.2564	0.3361	0.4138	0.6082		0.0171	0.2428	0.3183	0.3919	0.5759
0.7	0.0217	0.2901	0.3684	0.4460	0.6399		0.0205	0.2748	0.3489	0.4223	0.6059
0.8	0.0281	0.3308	0.4032	0.4799	0.6716		0.0266	0.3132	0.3818	0.4544	0.6360
(T^*)	n=0.1						Ceramic (n=0)				
	V=0	V=0.2	V=0.3	V=0.5	V=1		V=0	V=0.2	V=0.3	V=0.5	V=1
0.0	0.0000	0.0838	0.1255	0.1807	0.3190		0.0000	0.0716	0.1072	0.1544	0.2725
0.1	0.0015	0.1054	0.1519	0.2110	0.3588		0.0013	0.0900	0.1298	0.1803	0.3065
0.2	0.0028	0.1261	0.1782	0.2401	0.3948		0.0024	0.1078	0.1522	0.2051	0.3373
0.3	0.0051	0.1468	0.2044	0.2682	0.4278		0.0043	0.1255	0.1746	0.2292	0.3655
0.4	0.0075	0.1683	0.2307	0.2957	0.4582		0.0064	0.1438	0.1971	0.2527	0.3915
0.5	0.0107	0.1914	0.2573	0.3228	0.4868		0.0091	0.1635	0.2198	0.2758	0.4159
0.6	0.0153	0.2168	0.2841	0.3499	0.5142		0.0131	0.1852	0.2428	0.2989	0.4393
0.7	0.0183	0.2453	0.3115	0.3771	0.5410		0.0157	0.2096	0.2661	0.3221	0.4622
0.8	0.0238	0.2796	0.3409	0.4057	0.5678		0.0203	0.2389	0.2912	0.3466	0.4851

Fig. 4. Normalized temperature effects on nonlinear center deflection for various FGM indexes (V=0).
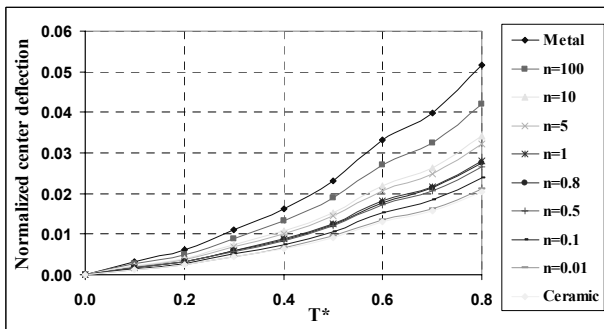

Fig. 5. Normalized temperature effects on nonlinear center deflection for various FGM indexes (V=0.2).

As demonstrated by the figures, the temperature field with the larger gradient will lead to greater deflections.

Figs. 6-8 depict the effect of FGM index on the non-linear thermo-electro-mechanical behavior (center deflection) of FGM plates with different normalized applied voltages (*V=0, 0.2, 1*) in logarithmic scale. It is also obvious from these figures that, by increasing the material gradients, the normalized center deflection would be increased in various temperature fields, and it is also demonstrated that larger thermal gradients will lead to greater deflections. This trend can be seen in various material gradients, which means that the non-linear deflection can be controlled by applying the appropriate voltage in the piezoelectric actuator layers.

We examine in this section the effect of control voltages and thermal environment on the vibration characteristics of the piezoelectric laminated circular FG plate for various FGM indexes. To this end, Table 4 as well as the Figs. 9-13 show the nonlinear relationships between the first natural frequencies $\omega_l a^2 \sqrt{I_1/D_2}$, versus the normalized temperature in various normalized control voltages V. These free vibrations are assumed to be in the vicinity of the nonlinearly deformed static equilibrium position.

Also, the effect of normalized temperature on the first natural frequency of the FG circular plate for various FGM indexes under various normalized control voltage is investigated and tabulated in Table 4, while the voltage-dependent first natural frequency changes are plotted in Figs. 9-13 for various temperatures. It is seen that the imposed voltage has a
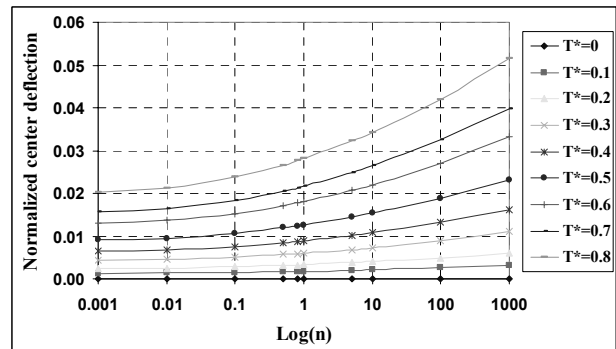

Fig. 6. FGM index effects on nonlinear center deflection for various normalized temperature (V=0).

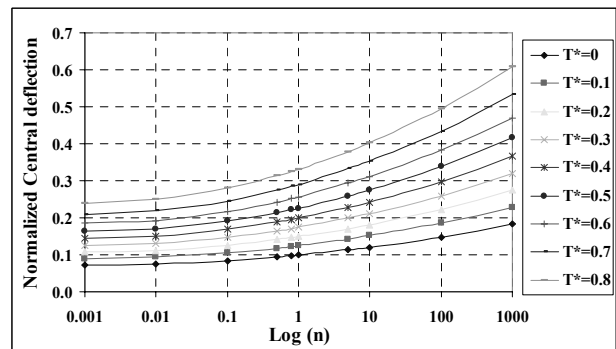

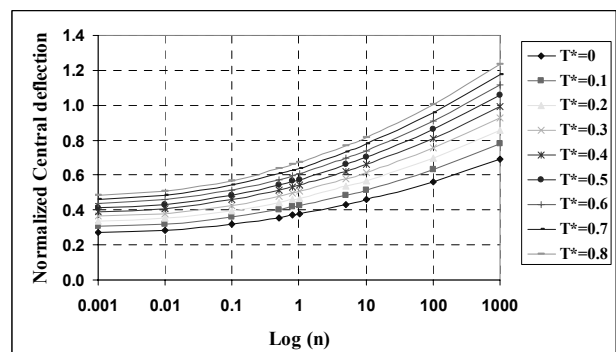Fig. 7. FGM index effects on nonlinear center deflection for various normalized temperature (V=0.2).

Fig. 8. FGM index effects on nonlinear center deflection for various normalized temperature (V=1).

significant effect on the first natural frequency of the structure, and by increasing the imposed voltage, the first natural frequency increases in a nonlinear manner. For instance, for the FGM plate with n=10 by increasing the imposed voltage from 0 to 0.2 the first natural frequency increases about 4.84%, while by increasing the voltage from 0.2 to 0.3 the first natural frequency increases about 15.12%.

It is seen that the imposed thermal environment has a significant effect on the first natural frequency of the structure, and by increasing the imposed temperature, the first natural frequency decreases in a nonlinear manner. However, this thermal tendency of decreasing the natural frequency can be

Table 4. FGM index and normalized temperature effects to the first natural frequency for various normalized voltages.

Normal-ized Voltage (V)	FGM index (n) / Normalized Temp. (T*)											
	Metal						n=10					
	Normalized Temperature (T*)						Normalized Temperature (T*)					
	-0.2	-0.1	0	0.2	0.5	0.8	-0.2	-0.1	0	0.2	0.5	0.8
0.0	5.3498	5.1218	4.8891	4.4249	3.5293	2.3669	6.0576	5.7994	5.5359	5.0103	3.9962	2.6800
0.2	5.4898	5.30304	5.1255	4.9006	4.68436	4.77695	6.2161	6.0046	5.8036	5.5490	5.3041	5.4089
0.4	5.7470	5.67268	5.5796	5.67452	5.92735	6.49712	6.5073	6.4232	6.3178	6.4253	6.7116	7.3567
0.3	6.0707	6.12308	6.1349	6.50337	7.06056	7.75663	6.8739	6.9332	6.9466	7.3638	7.9947	8.7829
0.8	6.4263	6.59038	6.7141	7.26308	8.00595	8.71889	7.2766	7.4623	7.6024	8.2240	9.0652	9.8724
1.0	6.7913	7.0417	7.2704	7.9106	8.7623	9.4951	7.6898	7.9733	8.2323	8.9572	9.9216	10.7513
1.2	7.1518	7.46439	7.7799	8.452	9.37002	10.1564	8.0980	8.4519	8.8092	9.5702	10.6097	11.5001
1.4	7.4999	7.85732	8.2352	8.91687	9.8835	10.7445	8.4922	8.8969	9.3247	10.0966	11.1911	12.1660
1.6	7.8317	8.22432	8.6394	9.33903	10.3511	11.2809	8.8679	9.3124	9.7824	10.5746	11.7206	12.7734
1.8	8.1454	8.56967	9.0016	9.74351	10.8027	11.7746	9.2230	9.7035	10.1925	11.0326	12.2319	13.3324
2.0	8.4404	8.8956	9.3329	10.1399	11.2449	12.2285	9.5571	10.0725	10.5677	11.4814	12.7326	13.8464
2.2	8.7175	9.20202	9.6436	10.5219	11.6637	12.6439	9.8708	10.4195	10.9195	11.9140	13.2069	14.3167
2.4	8.9784	9.48816	9.9414	10.8734	12.0351	13.0241	10.1663	10.7435	11.2567	12.3120	13.6274	14.7472
2.6	9.2275	9.75642	10.2302	11.1804	12.3427	13.3763	10.4484	11.0472	11.5837	12.6596	13.9757	15.1460
2.8	9.4727	10.0182	10.5104	11.4499	12.6036	13.7116	10.7259	11.3436	11.9010	12.9647	14.2711	15.5257
3.0	9.7277	10.3019	10.7796	11.7344	12.9013	14.0447	11.0147	11.6649	12.2058	13.2869	14.6082	15.9028

Table 4. Continued

Normalized Voltage (V)	FGM index (n) / Normalized Temp. (T*)											
	n=1						n=0.5					
	Normalized Temperature						Normalized Temperature					
	-0.2	-0.1	0	0.2	0.5	0.8	-0.2	-0.1	0	0.2	0.5	0.8
0.0	8.1105	7.7649	7.4121	6.7083	5.3506	3.5883	9.0587	8.6726	8.2786	7.4926	5.9761	4.0078
0.2	8.3228	8.0396	7.7704	7.4295	7.1017	7.2421	9.2957	8.9795	8.6788	8.2981	7.9319	8.0887
0.4	8.7127	8.6000	8.4589	8.6028	8.9861	9.8499	9.7313	9.6054	9.4478	9.6085	10.0366	11.0014
0.3	9.2035	9.2829	9.3008	9.8594	10.7041	11.7594	10.2794	10.3681	10.3881	11.0120	11.9555	13.1341
0.8	9.7426	9.9913	10.1789	11.0111	12.1374	13.2182	10.8816	11.1593	11.3689	12.2984	13.5563	14.7635
1.0	10.2959	10.6755	11.0222	11.9928	13.2840	14.3950	11.4995	11.9235	12.3108	13.3948	14.8370	16.0778
1.2	10.8424	11.3163	11.7947	12.8136	14.2054	15.3975	12.1099	12.6393	13.1735	14.3116	15.8660	17.1976
1.4	11.3702	11.9120	12.4849	13.5184	14.9838	16.2891	12.6995	13.3046	13.9444	15.0987	16.7355	18.1934
1.6	11.8732	12.4684	13.0977	14.1584	15.6927	17.1023	13.2613	13.9260	14.6289	15.8136	17.5273	19.1017
1.8	12.3487	12.9920	13.6468	14.7716	16.3774	17.8509	13.7923	14.5108	15.2422	16.4985	18.2920	19.9377
2.0	12.7960	13.4861	14.1491	15.3725	17.0478	18.5389	14.2919	15.0627	15.8032	17.1696	19.0407	20.7062
2.2	13.2160	13.9507	14.6201	15.9517	17.6827	19.1687	14.7610	15.5815	16.3293	17.8165	19.7499	21.4096
2.4	13.6117	14.3845	15.0716	16.4845	18.2458	19.7451	15.2030	16.0661	16.8335	18.4117	20.3788	22.0534
2.6	13.9893	14.7912	15.5094	16.9500	18.7121	20.2790	15.6248	16.5203	17.3226	18.9315	20.8996	22.6497
2.8	14.3610	15.1880	15.9342	17.3585	19.1076	20.7874	16.0398	16.9636	17.7970	19.3878	21.3413	23.2176
3.0	14.7476	15.6181	16.3423	17.7899	19.5589	21.2924	16.4717	17.4440	18.2528	19.8696	21.8455	23.7815

Table 4. Continued

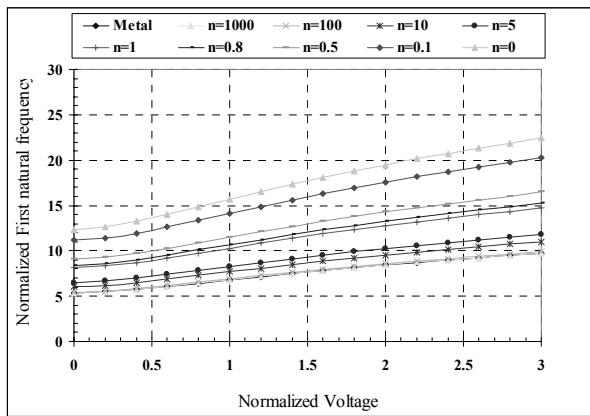| Normal-ized Volt-age (V) | FGM index (n) / Normalized Temp. (T*) | | | | | | | | | | | |
	n=0.1						Ceramic					
	Normalized Temperature						Normalized Temperature					
	-0.2	-0.1	0	0.2	0.5	0.8	-0.2	-0.1	0	0.2	0.5	0.8
0.0	11.1396	10.6649	10.1803	9.2138	7.3489	4.9285	12.3519	11.8255	11.2882	10.2165	8.1487	5.4648
0.2	11.4311	11.0423	10.6725	10.2043	9.7540	9.9468	12.6751	12.2440	11.8340	11.3148	10.8155	11.0293
0.4	11.9667	11.8120	11.6181	11.8158	12.3422	13.5287	13.2690	13.0974	12.8825	13.1017	13.6854	15.0009
0.3	12.6408	12.7498	12.7745	13.5417	14.7019	16.1513	14.0165	14.1373	14.1647	15.0154	16.3018	17.9090
0.8	13.3813	13.7228	13.9805	15.1236	16.6704	18.1549	14.8375	15.2162	15.5020	16.7694	18.4846	20.1307
1.0	14.1412	14.6626	15.1388	16.4719	18.2453	19.7712	15.6802	16.2583	16.7863	18.2645	20.2309	21.9228
1.2	14.8918	15.5427	16.1997	17.5992	19.5108	21.1482	16.5125	17.2342	17.9627	19.5145	21.6340	23.4497
1.4	15.6168	16.3609	17.1477	18.5672	20.5800	22.3728	17.3163	18.1414	19.0139	20.5878	22.8196	24.8075
1.6	16.3076	17.1251	17.9894	19.4462	21.5536	23.4897	18.0823	18.9888	19.9472	21.5625	23.8992	26.0460
1.8	16.9607	17.8442	18.7436	20.2885	22.4940	24.5178	18.8065	19.7861	20.7834	22.4964	24.9419	27.1860
2.0	17.5751	18.5229	19.4335	21.1138	23.4147	25.4628	19.4877	20.5387	21.5483	23.4116	25.9629	28.2339
2.2	18.1519	19.1609	20.0805	21.9093	24.2869	26.3278	20.1274	21.2462	22.2657	24.2936	26.9299	29.1929
2.4	18.6954	19.7568	20.7005	22.6412	25.0602	27.1195	20.7300	21.9068	22.9533	25.1051	27.7874	30.0708
2.6	19.2141	20.3153	21.3019	23.2804	25.7006	27.8527	21.3051	22.5262	23.6201	25.8140	28.4976	30.8839
2.8	19.7245	20.8604	21.8853	23.8416	26.2438	28.5511	21.8711	23.1306	24.2670	26.4362	29.0999	31.6582
3.0	20.2555	21.4512	22.4459	24.4340	26.8638	29.2446	22.4599	23.7856	24.8886	27.0931	29.7873	32.4272

Fig. 9. Effect of normalized voltage to first natural frequency for various FGM indexes (T*=-0.2).

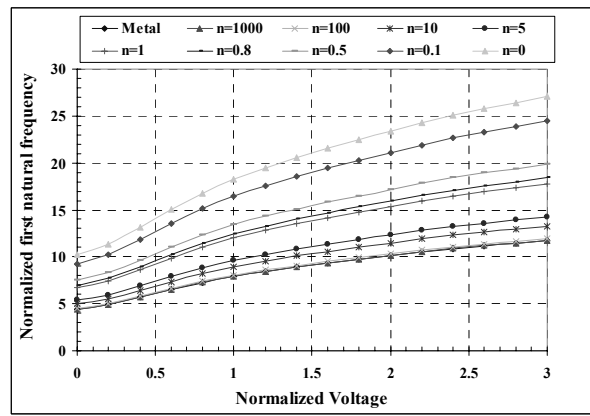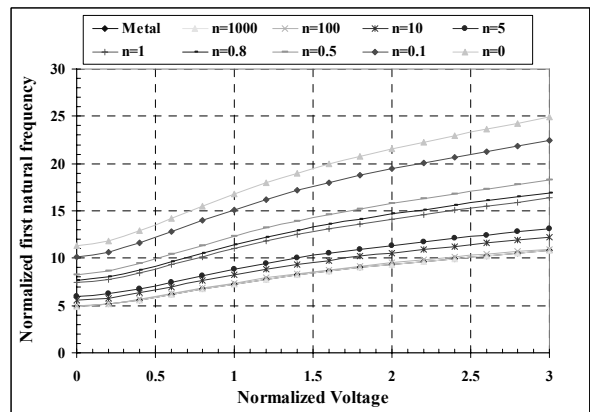Fig. 11. Effect of normalized voltage to first natural frequency for various FGM indexes (T*=0.2).

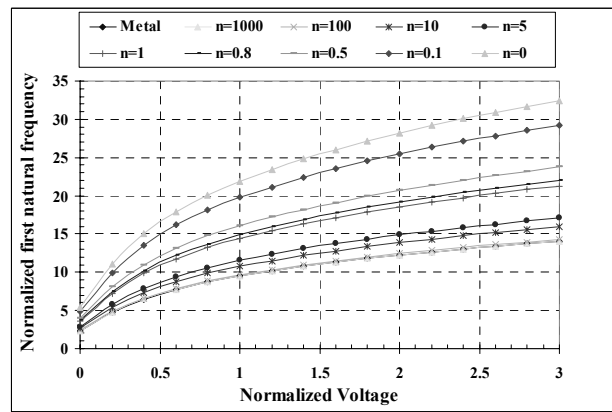Fig. 10. Effect of normalized voltage to first natural frequency for various FGM indexes (T*=0).

Fig. 12. Effect of normalized voltage to first natural frequency for various FGM indexes (T*=0.8).
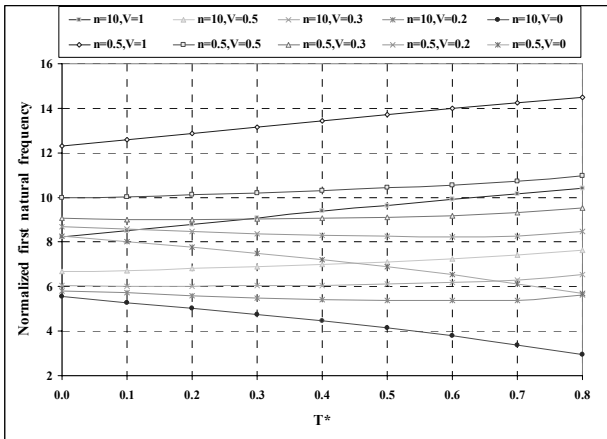
Fig. 13. Effects of normalized temperature on the normalized first natural frequency for various normalized voltages (n=10, n=0.5).
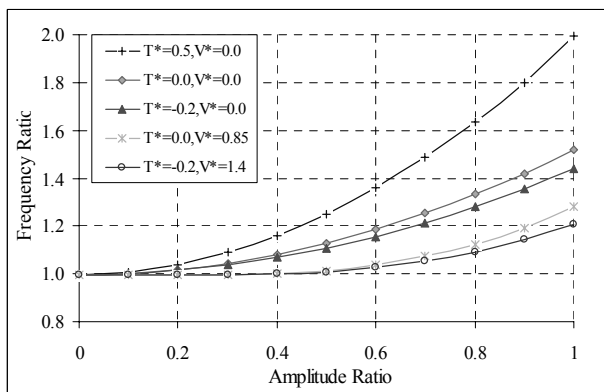

Fig. 14. Temperature/control effects on amplitude dependent first natural frequency (for metal plate) – amplitude ratio: w/h_f, frequency ratio: (ω/ω_1).

compensated and corrected with the control voltages V, as shown in Fig. 10-12.

Frequency variations of large amplitude oscillations with temperature and applied voltage changes are also investigated and plotted in Fig. 14. There are two sets of curves in this figure. The first set has no control voltages, and the second set has control voltages. It is observed that the control voltages actually reduce the nonlinear frequency and amplitude ratios, i.e., $P \rightarrow 1$. Accordingly, the nonlinear frequency and amplitude ratios can be actively controlled and the nonlinear effects reduced, i.e., the ratio is approaching to 1- the linear case. Other studies of the second natural frequency also suggest that the second natural frequency exhibits very much similar phenomena of the first natural frequency.

8. Summary and conclusions

A piezoelectric bounded circular FG plate subjected to temperature changes and control voltages is investigated based on classical plate theory, including the effects of the thermal gradient, piezothermoelasticity and von Karman type geometric

nonlinearity. Nonlinear coupled open-loop plate equations in radial and transverse oscillations were derived first, and then the equations were simplified to an axisymmetric oscillation case. An exact solution technique based on series-type solutions is used to obtain piezothermoelastic solutions for nonlinear static deformations and natural frequencies of the FG circular plate subjected to temperature and voltage excitations. Voltage controlled natural frequencies of the first mode at various temperatures are studied. It is observed that a higher temperature induces higher deflections of the plate, and the deflection at each temperature is attenuated when the control voltage increases, but this effect is predominant in higher voltages. Also by increasing the FGM gradient index the normalized center deflection will increase in a nonlinear manner in various temperature fields. It is seen that the imposed thermal environment has a significant effect on the natural frequency of the structure, and by increasing the imposed temperature, the natural frequency decreases in a nonlinear manner for various FGM indexes; this effect is predominant at higher temperatures. Both the nonlinear static deflections and natural frequencies are influenced by the temperatures and control voltages geometric and the static control voltages can be used to compensate nonlinear deflections.

References

[1] F. Peng, A. Ng and Y. R. Hu, Actuator placement optimization and adaptive vibration control of plate smart structures, *J. Intell. Mater. Syst. Struct.*, 16 (2005) 263-271.

[2] S. Dong and L. Tong, Vibration control of plates using discretely distributed piezoelectric quasi-modal actuators/sensors, AIAA *J.*, 39 (2001) 1766-1772.

[3] M. C. Ray, Optimal control of laminated shells with piezoelectric sensor and actuator layers, *AIAA J.*, 41 (2003) 1151-1157.

[4] W. J. Spencer, W. T. Corbett, L. R. Dominguez and B. D. Shafer, An electronically controlled piezoelectric insulin pump and valves, *IEEE Trans. Sonics Ultrason.*, 25 (1978) 153-156.

[5] S. Dong, X. Du, P. Bouchilloux and K. Uchino, Piezoelectric ring-morph actuation for valve application, *J. Electroceram.*, 8 (2002) 155-161.

[6] C. Y. K. Chee, L. Tong and G. P. Steve, A review on the modeling of piezoelectric sensors and actuators incorporated in intelligent structures, *J. Intell. Mater. Syst. Struct.,* 9 (1998) 3-19.

[7] L. Cao, S. Mantell and D. Polla, Design and simulation of an implantable medical drug delivery system using microelectromechanical systems technology, *Sensors Actuators A*, 94 (2001) 117-125.

[8] X. Chen, C. H. J. Fox and S. Mc William, Optimization of a cantilever microswitch with piezoelectric actuation, *J. Intell. Mater. Syst. Struct.,* 15 (2004) 823-834.

[9] J. N. Reddy and Z. Q. Cheng, Three-dimensional solutions of smart functionally graded plates, *ASME J. Appl. Mech.,* 68 (2001) 234-241.

[10] B. L. Wang and N. Noda, Design of smart functionally graded thermo-piezoelectric composite structure, *Smart Mater. Struct.,* 10 (2001) 189-193.

[11] X. Q. He, T. Y. Ng, S. Sivashanker and K. M. Liew, Active control of FGM plates with integrated piezoelectric sensors and actuators, *Int. J. Solids Struct.,* 38 (2001) 1641-1655.

[12] J. Yang, S. Kitipornchai and K. M. Liew, Nonlinear analysis of thermo-electro-mechanical behavior of shear deformable FGM plates with piezoelectric actuators, *Int. J. Numer. Methods Eng.,* 59 (2004) 1605-1632.

[13] X. L. Huang and H. S. Shen, Vibration and dynamic response of functionally graded plates with piezoelectric actuators in thermal environments, *J. Sound Vib.,* 289 (2006) 25-53.

[14] K. M. Liew, X. Q. He, T. Y. Ng and S. Kitipornchai, Finite element piezothermoelasticity analysis and the active control of FGM plates with integrated piezoelectric sensors and actuators, *Computational Mechanics,* 31 (2003) 350-358.

[15] P. C. Zhai, Q. J. Zhang and R. Z. Yuan, Influence of temperature dependent properties on temperature response and optimum design of C/M FGMs under thermal cyclic loading, *J. Wuhan Univ. Technol.* 12 (1997) 19-25.

[16] F. Ebrahimi and A. Rastgoo, Free vibration analysis of smart annular FGM plates integrated with piezoelectric layers, *Smart Mater. Struct.,* 17 (2008) No. 015044.

[17] F. Ebrahimi and A. Rastgoo, An analytical study on the free vibration of smart circular thin FGM plate based on classical plate theory, *Thin-Walled Structures,* 46 (2008) 1402-1408.

[18] F. Ebrahimi and A. Rastgoo, Free Vibration Analysis of Smart FGM Plates, *International Journal of Mechanical Systems Science and Engineering,* 2 (2) (2008) 94-99.

[19] F. Ebrahimi, A. Rastgoo and M. H. Kargarnovin, Analytical investigation on axisymmetric free vibrations of moderately thick circular functionally graded plate integrated with piezoelectric layers, *Journal of Mechanical Science and Technology,* 22 (6) (2008) 1056-1072.

[20] F. Ebrahimi, A. Rastgoo and A. A. Atai, Theoretical analysis of smart moderately thick shear deformable annular functionally graded plate, *European Journal of Mechanics - A/Solids,* 28 (2009) 962-997.

[21] F. Ebrahimi and A. Rastgoo, Nonlinear vibration of smart circular functionally graded plates coupled with piezoelectric layers, *Int J Mech Mater Des,* 5 (2009) 157-165.

[22] J. N. Reddy and G. N. Praveen, Nonlinear transient thermoelastic analysis of functionally graded ceramic-metal plate, *Int. J. Solids Struct.,* 35 (1998) 4457-4476.

[23] R. C. Wetherhold, S. Seelman and S.Wang, The use of functionally graded materials to eliminate or control thermal deformation, *Compos. Sci. Technol.,* 56 (1996) 1099-1104.

[24] Y. Tanigawa, H. Morishita and S. Ogaki, Derivation of system of fundamental equations for a three dimensional thermoelastic field with nonhomogeneous material properties and its application to a semi infinite body, *J. Therm. Stresses,* 22 (1999) 689-711.

[25] D. O. Brush and B. O. Almroth, *Buckling of Bars Plates and Shells,* McGraw-Hill, New York, (1975).

[26] J. N. Reddy, *Theory and Analysis of Elastic Plates,* Taylor and Francis, Philadelphia, (1999).

[27] G. Song, V. Sethi and H. N. Lic, Vibration control of civil structures using piezoceramic smart materials: A review, *Engineering Structures,* 28 (2006) 1513-1524.

[28] E. Efraim and M. Eisenberger, Exact vibration analysis of variable thickness thick annular isotropic and FGM plate, *J. Sound Vib.,* 299 (2007) 720-738.

[29] H. S. Tzou, Piezoelectric Shells-(Distributed Sensing and Control of Continua, Kluwer Dordrecht, (1993).

[30] X. J. Zheng and Y. H. Zhou, Analytical formulas of solutions of geometrically nonlinear equations of axisymmetric plates and shallow shells, *Acta Mech. Sinica,* 6 (1) (1990) 69-81.

[31] H. P. William, P. F. Brain and A. T. Sau, Numerical Recipes-the Art of Scientific Computing, Cambridge University Press, New York, (1986).

[32] H. Nayfe and D. T. Mook, *Nonlinear Oscillations,* John Wiley, New York, (1979).

Appendix A:

$$T_1 = T_2 + (T_U - T_L) - \frac{\kappa_c d + \kappa_m}{\kappa_m}(T_2 - T_L)$$

$$T_2 = T_L + \left[\frac{\kappa_m}{ch_f}(T_U - T_L)\right] \bigg/ \left[\frac{\kappa_p}{h_p} + \frac{\kappa_c d + \kappa_m}{ch_f}\right]$$

$$A_0 = T_2, \qquad A_1 = \frac{T_1 - T_2}{c}$$

$$A_2 = -\frac{T_1 - T_2}{c}\frac{\kappa_{cm}}{(N+1)\kappa_m}$$

$$A_3 = \frac{T_1 - T_2}{c}\frac{\kappa_{cm}^2}{(2N+1)\kappa_m^2}$$

$$A_4 = -\frac{T_1 - T_2}{c}\frac{\kappa_{cm}^3}{(3N+1)\kappa_m^3}$$

$$A_5 = \frac{T_1 - T_2}{c}\frac{\kappa_{cm}^4}{(4N+1)\kappa_m^4}$$

$$A_6 = -\frac{T_1 - T_2}{c}\frac{\kappa_{cm}^5}{(5N+1)\kappa_m^5}$$

where

$$\kappa_{cm} = \kappa_c - \kappa_m$$

$$c = 1 - \frac{1}{N+1}\frac{\kappa_{cm}}{\kappa_m} + \frac{1}{2N+1}\left(\frac{\kappa_{cm}}{\kappa_m}\right)^2 - \frac{1}{3N+1}\left(\frac{\kappa_{cm}}{\kappa_m}\right)^3$$

$$+ \frac{1}{4N+1}\left(\frac{\kappa_{cm}}{\kappa_m}\right)^4 - \frac{1}{5N+1}\left(\frac{\kappa_{cm}}{\kappa_m}\right)^5$$

$$d = 1 - \frac{\kappa_{cm}}{\kappa_m} + \left(\frac{\kappa_{cm}}{\kappa_m}\right)^2 - \left(\frac{\kappa_{cm}}{\kappa_m}\right)^3 + \left(\frac{\kappa_{cm}}{\kappa_m}\right)^4 - \left(\frac{\kappa_{cm}}{\kappa_m}\right)^5$$

Farzad Ebrahimi received his B.S. and M.S. in Mechanical Engineering from the University of Tehran, Iran. He is currently working on his Ph.D. thesis under the title of "Vibration analysis of smart functionally graded plates" at the Smart Materials and Structures Lab in the Faculty of Mechanical Engineering of the University of Tehran. His research interests include vibration analysis of plates and shells, smart materials and structures and functionally graded materials.